http://dx.doi.org/10.5935/0103-5053.20130169

J. Braz. Chem. Soc., Vol. 24, No. 8, 1339-1344, 2013.
Printed in Brazil - ©2013 Sociedade Brasileira de Química
0103 - 5053 $6.00+0.00

Article

Electrochemical Hydrogen-Storage Properties of $La_{0.78}Mg_{0.22}Ni_{2.67}Mn_{0.11}Al_{0.11}Co_{0.52}$-$M1Ni_{3.5}Co_{0.6}Mn_{0.4}Al_{0.5}$ Composites

Hongxia Huang,*[a,b] Guohui Li[a] and Shuxin Zhuang[c]

[a]*Guangxi Scientific Experiment Center of Mining, Metallurgy and Environment, College of Chemistry and Bioengineering, Guilin University of Technology, Guilin 541004, People's Republic of China*

[b]*Key Lab of New Processing Technology for Nonferrous Metals & Materials Ministry of Education, Guilin University of Technology, Guilin 541004, People's Republic of China*

[c]*School of Material Science and engineering, Xiamen University of Technology, Xiamen 361024, People's Republic of China*

Com o objetivo de aprimorar as propriedades eletroquímicas da liga do tipo AB_3 $La_{0,78}Mg_{0,22}Ni_{2,67}Mn_{0,11}Al_{0,11}Co_{0,52}$ como eletrodo negativo de bateria Ni–MH, seus compósitos relacionados $La_{0,78}Mg_{0,22}Ni_{2,67}Mn_{0,11}Al_{0,11}Co_{0,52}$–*x* wt.% $M1Ni_{3,5}Co_{0,6}Mn_{0,4}Al_{0,5}$ (*x* = 0, 10, 20, 30) foram preparados. A análise por difratometria de raios X (XRD) revelou que os compósitos consistem principalmente das fases $LaNi_5$ e La_2Ni_7. Apesar da pequena diminuição na capacidade de descarga máxima, o rendimento do ciclo foi significativamente melhorado. Experimentos de polarização linear (LP), polarização anódica (AP) e descarga de potencial degrau revelaram um aumento inicial da cinética eletroquímica que na sequência diminui com o aumento de *x*.

For improving the electrochemical properties of nonstoichiometric AB_3-type $La_{0.78}Mg_{0.22}Ni_{2.67}Mn_{0.11}Al_{0.11}Co_{0.52}$ alloy as negative electrode of Ni–MH battery, its related composites $La_{0.78}Mg_{0.22}Ni_{2.67}Mn_{0.11}Al_{0.11}Co_{0.52}$–*x* wt.% $M1Ni_{3.5}Co_{0.6}Mn_{0.4}Al_{0.5}$ (*x* = 0, 10, 20, 30) were prepared. Analysis by X-ray diffractometry (XRD) revealed that the composites consist mainly of $LaNi_5$ and La_2Ni_7 phases. Despite the small decrease in the maximum discharge capacity, the cycle performance was significantly enhanced. Linear polarization (LP), anodic polarization (AP) and potential step discharge experiments revealed that the electrochemical kinetics increases first and then decreases with increasing *x*.

Keywords: AB_3-type alloy, composite electrode material, cycle stability

Introduction

The discharge capacity of currently commercial AB_5-type hydrogen-storage alloys has reached 320-340 mAh g^{-1} at room temperature. It seems to be difficult to further improve the capacity of the AB_5-type alloys since the theoretical capacity of $LaNi_5$ is 372 mAh g^{-1}. Therefore, it is extremely important to develop new alloy types with higher capacity and longer life cycle for exacting the competition ability of Ni–MH batteries.

Recently, the new series of AB_3-type R–Mg–Ni-based (where R is a rare earth or Y, Ca) hydrogen-storage alloys were extensively investigated as promising candidates for negative electrode material of Ni–MH rechargeable batteries due to their relatively high hydrogen-storage capacity (360-410 mAh g^{-1}) and low production costs.[1] Dong *et al.*[2] reported that the $La_{0.67}Mg_{0.33}Ni_{2.75}Co_{0.25}$ alloy electrode exhibited a discharge capacity of 388 mAh g^{-1}, which was much higher than AB_5-type rare earth-based electrode alloys. However, these R–Mg–Ni-based alloys cannot meet the need of practical applications due to serious degradation of capacity during cyclic process.

Ball milling method is effective in the surface modification and improvement of the electrochemical properties of the hydrogen-storage alloys. For example, it was found that the maximum discharge capacity of $Ml_{0.90}Mg_{0.10}Ni_{3.08}Mn_{0.13}Co_{0.63}Al_{0.14}$–4 wt.% AB_5 electrode reached 406 mAh g^{-1} and that the $LaNi_5$ alloy could increase the discharge capacity of Ti–V-based BCC phase alloy.[3,4] Chu *et al.*[5] reported that the cyclic life of the $La_{0.7}Mg_{0.3}Ni_{3.5}$

*e-mail: hhxhunan@126.com

electrode was improved with addition of the $TiNi_{0.56}Co_{0.44}$ alloy.[6]

Herein, in order to obtain R–Mg–Ni-based hydrogen-storage alloys with excellent overall electrochemical properties, the $La_{0.78}Mg_{0.22}Ni_{2.67}Mn_{0.11}Al_{0.11}Co_{0.52}$–*x* wt.% $M1Ni_{3.5}Co_{0.6}Mn_{0.4}Al_{0.5}$ (where M1 denotes mischmetal, *x* = 0, 10, 20, 30) composites were prepared, which resulted in the appreciable elevation of the cycle stability. The microstructure and electrochemical properties of composites were also studied.

Experimental

Preparation and structural characterization

The $La_{0.78}Mg_{0.22}Ni_{2.67}Mn_{0.11}Al_{0.11}Co_{0.52}$ alloy (represented as A hereafter) and $M1Ni_{3.5}Co_{0.6}Mn_{0.4}Al_{0.5}$ alloy (represented as B hereafter, M1 consists of 37.7% La, 38.9% Ce, 6.3% Pr and 17.1% Nd) were prepared by induction melting under argon atmosphere and remelted four times for homogeneity. The purity of all the constituent metal elements was over 99.0%. The ingots were mechanically crushed and ground into 300 mesh powders for the preparation of the composite alloys. The A–*x* wt.% B (*x* = 0, 10, 20, 30) alloy and composites were prepared by ball milling. *x* wt.% (*x* = 0, 10, 20, 30) $M1Ni_{3.5}Co_{0.6}Mn_{0.4}Al_{0.5}$ alloy was mixed homogenously into $La_{0.78}Mg_{0.22}Ni_{2.67}Mn_{0.11}Al_{0.11}Co_{0.52}$ alloy, and ground by QM-ISP planetary ball miller under argon atmosphere for 1 h.

The structural data of the alloys was collected by powder X-ray diffraction (Rigaku D/max-2550, Cu K_α radiation, λ at 1.54178 Å).

Electrochemical measurements

The testing electrodes were prepared by cold pressing the alloy powder with carbonyl nickel powder in a weight ratio of 1:2 into a pellet of 15 mm in diameter under a pressure of 10 MPa and then pressed between two pieces of foam nickel. The charge/discharge studies were carried out by a Land 5.3 B Battery Test Instrument in a standard open tri-electrode electrolysis cell consisting of a working electrode (the MH pellet electrode for studying), a sintered $Ni(OH)_2$/NiOOH counter electrode, and a Hg/HgO reference electrode immersed in the 6 mol dm^{-3} KOH electrolyte. The electrodes were charged for 5 h at a current density of 100 mA g^{-1}, rested for 5 min and then discharged to the cut-off potential of –0.6 V *vs.* Hg/HgO reference electrode at a current density of 50 mA g^{-1}.

PARSTAT 2273 electrochemical system was used for the kinetic tests. The anodic polarization was plotted at a rate of 0.5 mV s^{-1} from 0 to 600 mV (*vs.* open circuit potential) at 50% depth of discharge (DOD). The linear polarization testing was performed at a rate of 0.1 mV s^{-1} from –5 to 5 mV (*vs.* open circuit potential) at 50% DOD. Electrochemical impedance spectroscopy measurement was carried out in the frequency range of 1×10^3 to 1×10^{-4} Hz with ac amplitude of 5 mV at 50% DOD. The potential step discharge experiments were performed at 100% charge state, a +500 mV potential step was applied and the discharge time was 3600 s.

Results and Discussions

Phase structure

Figure 1 exhibits the XRD patterns for B, *x* = 0 and *x* = 10 alloys. It shows that the $M1Ni_{3.5}Co_{0.6}Mn_{0.4}Al_{0.5}$ alloy presents the single $CaCu_5$-type hexagonal $LaNi_5$ phase. The *x* = 0 and the *x* = 10 alloys consist of multiphase structures, the main phases are $LaNi_5$ and La_2Ni_7 phases, indicating that the crystal structure of the alloy is not affected by appropriate milling.

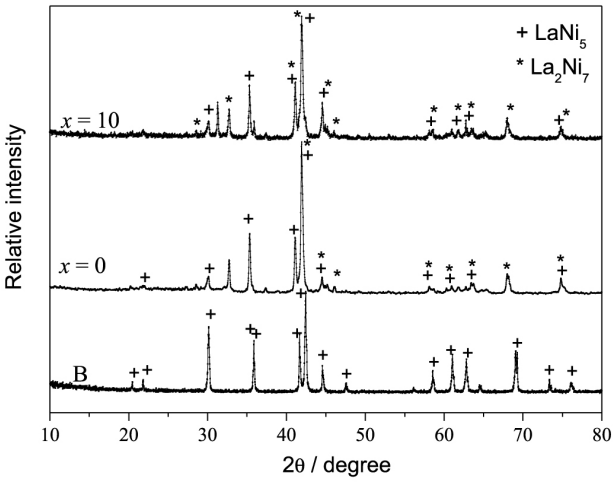

Figure 1. X-ray diffraction patterns for the B, *x* = 0 and *x* = 10 alloys.

Discharge capacity and cycle stability

Figure 2 illustrates the discharge capacity *vs.* cycle number for the A–*x* wt.% B (*x* = 0, 10, 20, 30) alloy electrodes. For comparison, the same relationship for the $M1Ni_{3.5}Co_{0.6}Mn_{0.4}Al_{0.5}$ alloy (represented as B) is also presented. The activation number (N_a) and the maximum discharge capacity (C_{max}) are listed in Table 1. The activation capability is closely related to the phase structure, surface characteristics, grain size and interstitial dimensions of the alloy. It is obvious that all the composite electrodes have excellent activation property and can be

Table 1. The electrochemical properties of the A–*x* wt% B (*x* = 0, 10, 20, 30) alloy electrodes.

Alloy	N_a	C_{max} / (mAh g^{-1})	C_{50th} / (mAh g^{-1})	S_{50} / %	I_0 / (mA g^{-1})	I_L / (mA g^{-1})	D / (× 10^{-10} cm^2 s^{-1})	HRD_{600} / %
B	4	315	279	88.6	77.0	443.4	1.33	83.7
x = 0	3	371	205	55.3	191.6	1204.0	2.24	84.2
x = 10	1	369	239	64.8	282.9	1639.6	4.01	95.8
x = 20	2	358	274	76.5	255.6	1481.9	2.56	94.2
x = 30	2	356	261	73.1	237.0	1358.4	2.33	88.8

fully activated within three cycles, being mainly ascribed to their multiphase structures. The phase boundary cannot only act as a buffer for releasing strain energy but also provides good tunnels for the diffusion of hydrogen atoms, which was confirmed by literature.[7]

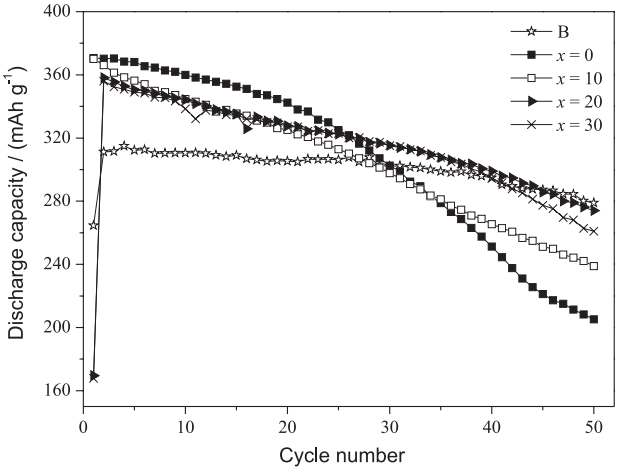

Figure 2. Evolution of the discharge capacities of the A–*x* wt.% B (*x* = 0, 10, 20, 30) with the cycle number.

The oxidation and corrosion of the alloy composition in corrosive electrolyte is an extremely important factor that leads to the efficacy loss of the Ni–MH battery. In order to investigate the cycling durability of the alloy electrodes, the capacity retention (S_n) is defined and calculated by the following equation:

$$S_n\,(\%) = C_{nth}/C_{max}\ 100 \qquad (1)$$

where S_n is the capacity retention at *n* cycles, C_{nth} is the discharge capacity at *n* cycles and C_{max} is the maximum discharge capacity. The capacity retention rate at the 50th cycle (S_{50}) of the alloy electrodes is shown in Table 1.

C_{max} of the $M1Ni_{3.5}Co_{0.6}Mn_{0.4}Al_{0.5}$ alloy electrode is 315 mAh g^{-1}, and the capacity retention (S_{50}) is 88.6%. With a maximum discharge capacity of 371 mAh g^{-1} for *x* = 0 electrode, its cycle stability is rather poor. After 50 cycles, S_{50} is only 55.3%. As for the composite electrodes, C_{max} decreases to 369 mAh g^{-1} (*x* = 10), 358 mAh g^{-1} (*x* = 20) and 356 mAh g^{-1} (*x* = 30), respectively. The hydrogen-storage capacity of the La_2Ni_7 phase is higher than that of $LaNi_5$ phase,[8] so the drop of the maximum discharge capacity can be attributed to the abundance decrease of the La_2Ni_7 phase with the addition of $M1Ni_{3.5}Co_{0.6}Mn_{0.4}Al_{0.5}$ alloy.

The cycle stability of the composite electrodes is significantly elevated, especially for *x* = 20 electrode, which exhibits the capacity retention rate (S_{50}) of 76.5%. The improvement of the cycle performance is related to the change of the phase abundances of the alloys. The abundance of $LaNi_5$ phase increases with the addition of $M1Ni_{3.5}Co_{0.6}Mn_{0.4}Al_{0.5}$ alloy, which is beneficial to the improvement of the cycle stability owing to the high Ni content of $LaNi_5$ phase. Ni has excellent electrocatalytic activity and good corrosion resistance in an alkaline solution.[9]

Anodic polarization (AP)

Figure 3 shows the anodic polarization curves for the A–*x* wt.% B (*x* = 0, 10, 20, 30) alloy electrodes at 50% DOD. The anodic current density increases firstly with the overpotential increase, and then reaches a limiting value defined as the limiting current density (I_L), which is mainly controlled by the hydrogen diffusion in the bulk of alloy. The hydrogen diffusion is higher as the limiting current density is larger. The values of I_L obtained from Figure 3 are also summarized in Table 1. I_L increases from 1204.0 mA g^{-1} (*x* = 0) to 1639.6 mA g^{-1} (*x* = 10), and then decreases to 1358.4 mA g^{-1} (*x* = 30). Liu *et al.*[10] reported that the kinetics may be affected by the relative content of the two phases in the alloys. When the relative content of the $LaNi_5$ and La_2Ni_7 phases come to a proper value, the electrochemical catalytic-activity of the alloy electrodes is enhanced due to the synergy of the two phases.[11] Therefore, I_L increases and then decreases with the *x* increase.

Linear polarization (LP)

Figure 4 illustrates the linear polarization curves for the A–*x* wt.% B (*x* = 0, 10, 20, 30) alloy electrodes. When the overpotential is changed within a small range, there is

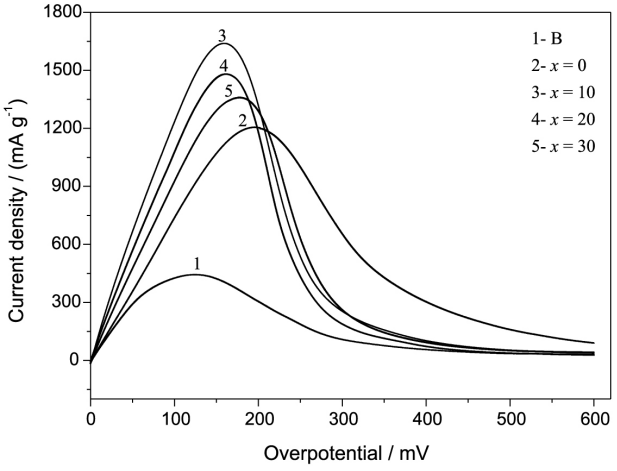

Figure 3. Anodic polarization curves for the A–*x* wt.% B (*x* = 0, 10, 20, 30) alloy electrodes at 50% DOD (scan rate: 0.5 mV s^{-1}).

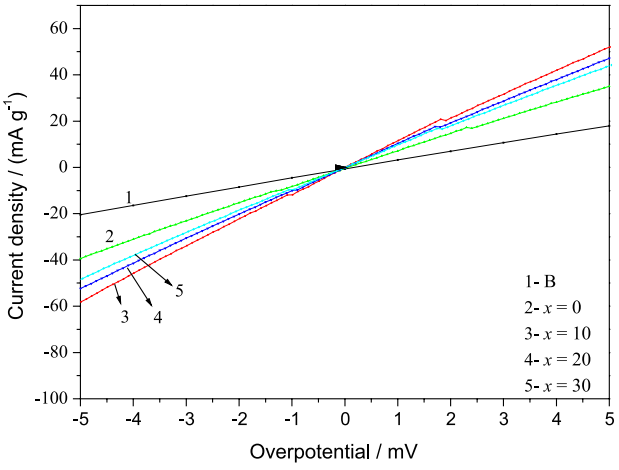

Figure 4. Linear polarization curves for the A–*x* wt.% B (*x* = 0, 10, 20, 30) alloy electrodes at 50% DOD (scanning rate: 0.1 mV s^{-1}).

a good linear dependence between the current density and the overpotential. The exchange current density (I_0) is an important kinetic parameter, which is used to evaluate the charge-transfer reaction rate on the electrode surface and can be calculated by the following equation:[12]

$$I_0 = \frac{R\,T\,I_d}{F\,\eta} \qquad (2)$$

where I_d, R, T, F and η denote the applied current density, gas constant, absolute temperature, Faraday constant and overpotential, respectively. As listed in Table 1, I_0 increases after addition of $M1Ni_{3.5}Co_{0.6}Mn_{0.4}Al_{0.5}$ alloy, which is related to the change in the abundance of $LaNi_5$ phase. The $LaNi_5$ phase has higher electrocatalytic activity due to its higher Ni content, which cannot only work as a hydrogen absorber, but also as a catalytic site during the charge/discharge process.[13] The exchange current density of the electrodes firstly increases from 191.6 mA g^{-1} (x = 0) to 282.9 mA g^{-1} (x = 10), and then decreases to 237.0 mA g^{-1} (x = 30) with the increase of x value. The variation of I_0 is completely consistent with that of I_L, which further confirms that the alloy electrode exhibits a comparatively better kinetics when the La_2Ni_7 and $LaNi_5$ phases exist in a proper proportion.

Potentiostatic discharge

Figure 5 shows the curves of anodic current *vs.* discharge time curves for the A–*x* wt.% B (*x* = 0, 10, 20, 30) alloy electrodes at full charge state. It can be seen that after application of the overpotential, the current-time responses in the semilogarithmic plot (log *i vs. t*) can be divided into two domains. In the first region, the current density decreases rapidly due to the fast consumption of the hydrogen on the surface of the alloy particles, while the current density decreases slowly in a linear fashion in the second region. In the second region, the current is mainly controlled by the hydrogen diffusion velocity, and the hydrogen is supplied from the bulk alloy proportionally to the concentration gradient of hydrogen. According to a spherical diffusion model,[14] the hydrogen diffusion coefficient (D) can be obtained from the slope of the linear section by the following equations:[15]

$$\log i = \log\left(\frac{6\,F\,D}{d\,a^2}(C_0 - C_s)\right) - \frac{\pi^2}{2.303}\frac{D}{a^2}t \qquad (3)$$

$$D = -\frac{2.303\,a^2}{\pi^2}\frac{\mathrm{d}\log i}{\mathrm{d}t} \qquad (4)$$

where D, C_0, C_s, a, d, t and i denote the average coefficient of diffusion of hydrogen (cm^2 s^{-1}), the initial hydrogen

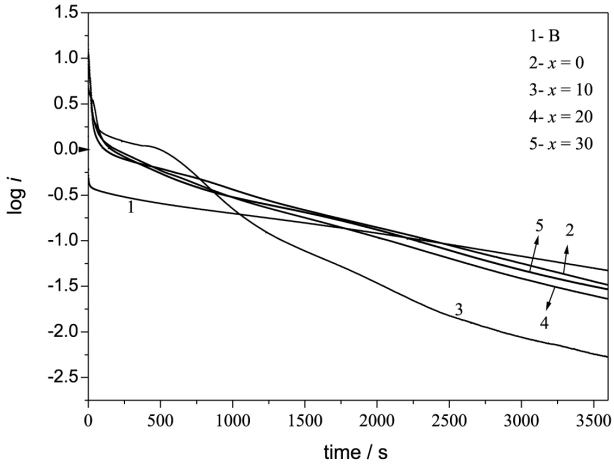

Figure 5. Semilogarithmic curves of anodic current *vs.* time for the A–*x* wt.% B (*x* = 0, 10, 20, 30) alloy electrodes at full charge state (+500 mV potential step).

concentration in the bulk of the alloy (which is considered uniform, mol cm^{-3}), the hydrogen concentration on the surface of the alloy particles (which is considered uniform, mol cm^{-3}), the alloy particle radius (cm), the density of the hydrogen-storage alloys (g cm^{-3}), the discharge time (s) and the diffusion current density (A g^{-1}), respectively. With an assumed average particle radius of a = 15 μm, the values of D calculated by the equation 4 are tabulated in Table 1. The hydrogen diffusion coefficient increases from 2.24×10^{-10} $cm^2 s^{-1}$ (x = 0) to 4.01×10^{-10} $cm^2 s^{-1}$ (x = 10), and then decreases to 2.33×10^{-10} $cm^2 s^{-1}$ (x = 30). It indicates that the hydrogen diffusivity firstly increases and then drops with the addition of AB_5-type $M1Ni_{3.5}Co_{0.6}Mn_{0.4}Al_{0.5}$ alloy, in agreement with the limiting current density.

Electrochemical impedance spectra (EIS)

The charge-transfer resistance (R_{ct}) of the alloy electrode can be determined by the electrochemical impedance spectra. Figure 6 illustrates the EIS curves for the A–x wt.% B (x = 0, 10, 20, 30) alloy electrodes at 50% DOD. It can be seen that each spectrum consists of a smaller semicircle in the high-frequency region and a larger semicircle in the low-frequency region followed by a straight line. According to the study of Kuriyama *et al*.,[16] the high-frequency semicircle represents the contact resistance between the current collector and the alloy electrode, the low-frequency semicircle represents the charge-transfer resistance, and the straight line is namely Warburg impedance. It can be seen in Figure 6 that the contact impedance remains almost unchanged, but the radius of the large arc in the low-frequency region is in the order of $x = 0 > x = 30 > x = 20 > x = 10$, indicating that the charge-transfer resistance increases firstly and then decreases with increasing x, and the electrode with x = 10 exhibits the best electrochemical reaction rate.

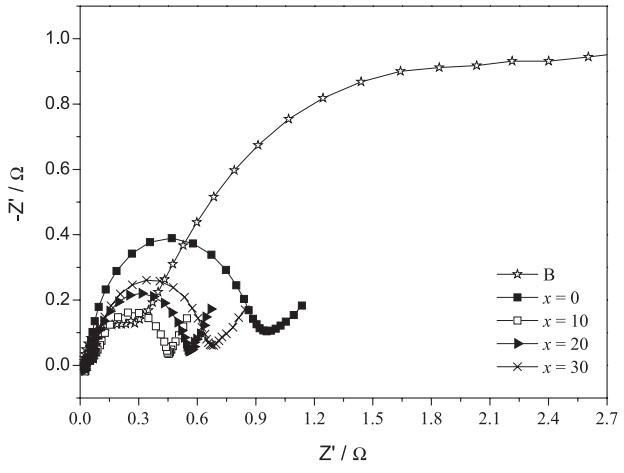

Figure 6. The electrochemical impedance spectra for the A–x wt.% B (x = 0, 10, 20, 30) alloy electrodes at 50% DOD (open circuit potential, amplitude 5 mV).

High rate dischargeability (HRD)

Figure 7 presents the high rate dischargeability for the A–x wt.% B (x = 0, 10, 20, 30) alloy electrodes. The value of HRD is calculated according to the following equation:

$$\text{HRD}\ (\%) = C_d/C_{50}\ 100 \qquad (5)$$

where C_d and C_{50} represent the discharge capacities at the current densities of I_d and 50 mA g^{-1}, respectively. The values with the discharge current density of 600 mA g^{-1} are listed in Table 1. The $M1Ni_{3.5}Co_{0.6}Mn_{0.4}Al_{0.5}$ alloy presents the single $LaNi_5$ phase, and the A–x wt.% B (x = 0, 10, 20, 30) alloys consist of multiphase structures. The phase boundary may decrease the lattice distortion and strain energy. Moreover, the phase boundary can provide good tunnels for the diffusion of hydrogen atoms, therefore, the kinetics of A–x wt.% B (x = 0, 10, 20, 30) is improved. For the composite electrodes, the HRD_{600} value increases from 84.2 % (x = 0) to 95.8% (x = 10), and then decreases to 88.8% (x = 30). It is well known that HRD is closely related to the kinetics of the alloy, which is mainly controlled by both the charge transfer resistance at the surface of alloy electrode and the hydrogen diffusion resistance inside the bulk of alloy.[17] A proper ratio of La_2Ni_7 to $LaNi_5$ phases is probably the reason why the electrode with x = 10 presents the best kinetic performance.

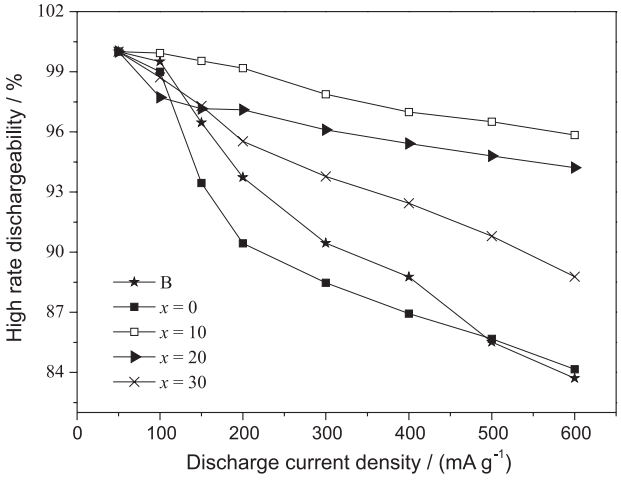

Figure 7. The high rate dischargeability for the A–x wt.% B (x = 0, 10, 20, 30) alloy electrodes.

Figure 8 shows HRD_{600} as a function of I_0 (obtained from linear polarization) for the A–x wt.% B (x = 0, 10, 20, 30) alloy electrodes. There is a linear relationship between

HRD_{600} and I_0. It is accepted that in case the charge-transfer reaction on the surface of the alloy electrodes is the rate-determining factor, a linear dependence of the HRD on the exchange current density would be obtained.[18] Accordingly, it is concluded that the HRD is essentially controlled by electrochemical reaction of hydrogen on alloy surface at the discharge current density of 600 mA g^{-1}.

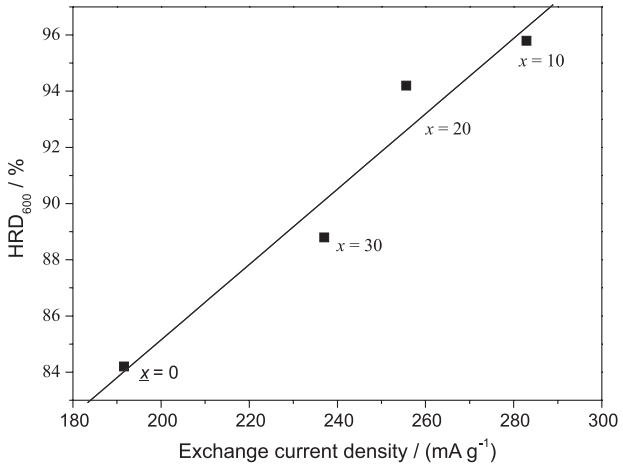

Figure 8. Dependence of HRD_{600} on I_0 of the A–*x* wt.% B (*x* = 0, 10, 20, 30) alloy electrodes.

The electrochemical kinetics is mainly determined by both the charge-transfer resistance on the surface of alloy electrode and hydrogen atom diffusion within the bulk of the alloy. The former can be characterized by I_0 or R_{ct}, while the latter can be characterized by the hydrogen diffusion coefficient or the limiting current density. In the present study, I_0, I_L and *D* firstly increase and then decrease with increasing *x* from 0 to 30. Thus, the kinetics of the investigated electrodes increases and then decreases with the increasing of $M1Ni_{3.5}Co_{0.6}Mn_{0.4}Al_{0.5}$ alloy content.

Conclusions

The $La_{0.78}Mg_{0.22}Ni_{2.67}Mn_{0.11}Al_{0.11}Co_{0.52}$–*x* wt.% $M1Ni_{3.5}Co_{0.6}Mn_{0.4}Al_{0.5}$ (*x* = 0, 10, 20, 30) composite alloys have a multi-phase structure of $LaNi_5$ and La_2Ni_7 phases. With the addition of $M1Ni_{3.5}Co_{0.6}Mn_{0.4}Al_{0.5}$ alloy, the discharge capacity slightly drops, while the cycle stability is obviously enhanced. The kinetics of alloy electrodes firstly increases and then decreases with *x* increase. The linear relationship between HRD and I_0 indicates that charge-transfer reaction on the surface should be the rate-determining factor for the electrochemical kinetics when the discharge current density is 600 mA g^{-1}.

Acknowledgements

This work was financially supported by the Education Department and Scientific Foundation of Guangxi (201203YB088).

References

1. Zhang, Y. H.; Dong, X. P.; Li, B. W.; Ren, H. P.; Wu, Z. W.; Wang, X. L.; *J. Alloys Compd*. **2008**, *465*, 422.
2. Dong, Z. W.; Wu, Y. M.; Ma, L. Q.; Wang, L. D.; Shen, X. D.; Wang, L. M.; *Int. J. Hydrogen Energy* **2011**, *36*, 3050.
3. Hu, L.; Han, S. M.; Li, J. H.; Zhu, X. L.; Li, Y.; *Rare Met*. **2008**, *27*, 429.
4. Yu, X. B.; Walker, G. S.; Grant, D. M.; Wu, Z.; Xia, B. J.; Shen, J.; *Appl. Phys. Lett*. **2005**, *87*, 133121.
5. Chu, H. L.; Qiu, S. J.; Sun, L. X.; Zhang, Y.; Xu, F.; Zhu, M.; Hu, W. Y.; *Int. J. Hydrogen Energy* **2008**, *33*, 755.
6. Huang, H. X.; Huang, K. L.; Chen, D. Y.; Li, S. Q.; Zhuang, S. X.; *J. Mater. Sci*. **2010**, *45*, 1123.
7. Zhang, Y. H.; Li, B. W.; Ren, H. P.; Cai, Y.; Dong, X. P.; Wang, X. L.; *Int. J. Hydrogen Energy* **2007**, *32*, 4627.
8. Oesterreicher, H.; Clinton, J.; Bittner, H.; *Mater. Res. Bull*. **1976**, *11*, 1241.
9. Wang, Y.; Wang, X.; Gao, X. P.; Shen, P. W.; *Int. J. Hydrogen Energy* **2007**, *32*, 4180.
10. Liu, Y. F.; Jin, Q. W.; Gao, M. X.; Zhu, Y. F.; Zhang, Z. H.; Pan, H. G.; *Rare Met. Mater. Eng*. **2003**, *32*, 942.
11. Zhang, Z.; Han, S. M.; Li, Y.; Jing, T. F.; *J. Alloys Compd*. **2007**, *431*, 208.
12. Notten, P. H. L.; Hokkeling, P.; *J. Electrochem. Soc*. **1991**, *138*, 1877.
13. Li, Y.; Han, S. M.; Li, J. H.; Hu, L.; *Electrochim. Acta* **2007**, *52*, 5945.
14. Nishima, T.; Ura, H.; Uchida, I.; *J. Electrochem. Soc*. **1997**, *144*, 1273.
15. Zheng, G.; Popov, B. N.; White, R. E.; *J. Electrochem. Soc*. **1995**, *142*, 2695.
16. Kuriyama, N.; Sakai, T.; Miyamura, H.; Uehara, I.; Ishikawa, H.; Iwasaki, T.; *J. Alloys Compd*. **1993**, *202*, 183.
17. Li, Y.; Han, S. M.; Li, J. H.; Zhu, X. L.; Hu, L.; *J. Alloys Compd*. **2008**, *458*, 357.
18. Iwakura, C.; Oura, T.; Inoue, H.; Matsuoka, M.; *Electrochim. Acta* **1996**, *41*, 117.

Submitted: February 17, 2013
Published online: July 12, 2013